

Integrating remote sensing into forest ecosystem modeling through Bayesian calibration

Journal:	<i>International Journal of Remote Sensing</i>
Manuscript ID:	TRES-SIP-2006-0033
Manuscript Type:	Special Issue Paper
Date Submitted by the Author:	09-Oct-2006
Complete List of Authors:	Patenaude, Genevieve; University of Edinburgh, School of Geosciences Milne, Ronald; Centre for Ecology and Hydrology, Edinburgh Van Oijen, Marcel; Centre for Ecology and Hydrology, Edinburgh Rowland, Clare; Centre for Ecology and Hydrology, Section for Earth Observation Hill, Ross; Centre for Ecology and Hydrology, Section for Earth Observation
Keywords:	FORESTRY, HYPERSPECTRAL DATA, LIDAR, SAR
Keywords (user defined):	Bayesian, Uncertainty, Ecological modelling



1 **Abstract**

2 Process-based models have been used to simulate 3 dimensional complexities of
3 forest ecosystems and their temporal changes but their extensive data requirement and
4 complex parameterisation has often limited their use for practical management
5 applications. Increasingly, information retrieved with remote sensing techniques can
6 help in model parameterisation and data collection by providing spatially and
7 temporally resolved forest information. In this paper, we illustrate the potential of
8 Bayesian calibration for integrating such data sources to simulate forest production.
9 As an example, we use the 3-PG model combined with hyperspectral, LiDAR, SAR
10 and field-based data to simulate the growth of UK Corsican pine stands.
11 Hyperspectral, LiDAR and SAR data are used to estimate LAI dynamics, tree height
12 and above ground biomass respectively, while the Bayesian calibration provides
13 estimates of uncertainties to model parameters and outputs. The Bayesian calibration
14 contrasts with goodness-of-fit approaches which do not provide uncertainties to
15 parameters and model outputs. Parameters and the data used in the calibration process
16 are presented in the form of probability distributions, reflecting our degree of certainty
17 about them. After the calibration, the distributions are updated. To approximate
18 posterior distributions (of outputs and parameters), a Markov Chain Monte Carlo
19 sampling approach is used (25000 steps). A sensitivity analysis is also conducted
20 between parameters and outputs. Overall, the results illustrate the potential of a
21 Bayesian framework for truly integrative work, both in the consideration of field-
22 based and remotely sensed datasets available and in estimating parameter and model
23 output uncertainties.

24

1 Introduction

Process-based models are widely used in the fields of forest physiology and forest ecology as they enable deeper insights into the drivers of forest production and growth and offer higher flexibility than conventional production tables (Landsberg & Waring 1997). This flexibility enables the quantification and prediction of forest 2 and 3-D structural variables owing to deterministic, mechanistic and/or stochastic algorithms simulating the processes affecting growth. However, their practical value has often been limited owing to (a) their extensive data requirement and (b) their complexity and the difficulty in quantifying parameters and model output uncertainty (e.g. Gertner et al. 1999).

Remote sensing technology is increasingly exploited for forest inventorying and monitoring (e.g. Baulies and Pons 1995, Hyypä et al. 2000) as it can provide insights into the spatial and temporal variability of forests, information which is seldom available from ground surveys alone. While it is a generally accepted premise that field data provide the closest representation of reality, spatially resolved ground based data can be time consuming, expensive and logistically difficult to acquire where access to forested land is limited. Comparatively, highly resolved remote sensing data can be obtained at relatively low costs. Additionally, novel approaches now supply estimates of forest structural variables of accuracy equivalent if not superior to traditional measurements techniques (e.g. Magnussen and Boudewyn 1998, Hyypä *et al.* 2001). Remote sensing may therefore help meet forest ecophysiologicals and modellers' data requirements.

1
2
3
4 49 In this context, we present Bayesian calibration (BC) as a means to integrate remotely
5
6 50 acquired datasets into ecological models. This approach offers a number of
7
8 51 advantages in comparison with goodness-of-fit and optimisation approaches. In
9
10 52 addition to facilitating the integration of data of varying degree of uncertainty, BC
11
12 53 enables the quantification of uncertainty associated with parameters and model
13
14 54 outputs, an important requirement for practical applications of models (Green *et al.*
15
16 55 2000). Parameters and data used in the calibration process are presented in the form
17
18 56 of probability distributions, reflecting our degree of certainty about them (Jansen
19
20 57 1999). Bayesian calibration enables the updating of distributions as further
21
22 58 information is gained. The framework thereby targets the much-needed platform for
23
24 59 (i) integrating datasets of varying degree of certainty and (ii) expressing parameter
25
26 60 and output uncertainty in forest-growth modelling (Green *et al.* 2000, Ghazoul &
27
28 61 McAllister 2003, Van Oijen *et al.* 2005).
29
30
31
32
33
34
35

36
37 63 In this paper, we demonstrate the usefulness of the approach by calibrating the 3-PG
38
39 64 model (Physiological Processes Predicting Growth, Landsberg & Waring 1997, Sands
40
41 65 & Landsberg 2002) for UK Corsican pine stands (*Pinus nigra* *car. maritima* (AIT.)
42
43 66 Melv.). 3-PG is built on a combination of process-based calculations, several key
44
45 67 simplifying assumptions and few empirical relationships. The model predicts gross
46
47 68 and net primary production as well as biomass allocation to different pools. Over the
48
49 69 years, it has been increasingly and successfully been applied to new species
50
51 70 worldwide (Landsberg & Waring 1997, Law *et al.* 2000, Waring 2000, Coops &
52
53 71 Waring 2001, Coops *et al.* 2001, Sands & Landsberg 2002, Almeida *et al.* 2004, Stape
54
55 72 *et al.* 2004). However, the parameterisation of the model for new species remains a
56
57 73 challenge. As stated by Sands (2004, p.3): "In only a few cases have parameters
58
59
60

1
2
3
4 74 characterising a species been rigorously determined, and even then this has been
5
6 75 largely by a process of trial and error”. In this context, the aim of this paper is to
7
8 76 illustrate the potential of BC as a means to (i) calibrate models for novel species (ii)
9
10 77 integrate multi-source datasets and (iii) quantify model parameters and outputs along
11
12 78 with uncertainty.
13
14

15 79
16
17 80 Our paper is structured as follow. In section two, we present an overview of the 3-PG
18
19 81 principal submodels. Section three provides a description of the field site, available
20
21 82 remote sensing and field based datasets for model initialisation, parameterisation and
22
23 83 calibration. The processing of the databases is also briefly summarised. Section four
24
25 84 contains the description of the Bayesian calibration and finally, results and
26
27 85 discussions are presented in section five and six, respectively.
28
29
30
31

32 86 33 34 87 **2 Structure of the 3-PG model**

35
36 88 The 3-PG model has monthly or annual time steps and entails five state variables –
37
38 89 foliage, stem and root biomass, stocking density and available soil water – in
39
40 90 conjunction with five submodels –biomass production; biomass allocation; soil water
41
42 91 availability and evapotranspiration; mortality; and inventory variables. The required
43
44 92 climatic data are monthly average values of solar radiation ($\text{MJ m}^{-2} \text{d}^{-1}$), atmospheric
45
46 93 water pressure deficit (mbar), mean air temperature ($^{\circ}\text{C}$), rainfall (mm month^{-1}) and
47
48 94 frost days. Other input variables include site latitude, an estimate of soil fertility,
49
50 95 maximum available soil water (mm per depth of rooting zone, in meters) and a
51
52 96 general description of soil texture. 3-PG outputs considered in this study were leaf
53
54 97 area index (LAI, projected), above ground biomass (ABG biomass, t ha^{-1}), stem
55
56 98 biomass (t ha^{-1}), foliage biomass (t ha^{-1}), root biomass (t ha^{-1}) and stem height (m).
57
58
59
60

2.1 Biomass production

The biomass submodel converts solar radiation into dry matter. The interception of radiation is defined by Beer's law and canopy LAI. The amount of photosynthetically active radiation intercepted by a stand (ϕ_{pa} , mol MJ⁻¹) is then converted into carbohydrates by means of a canopy quantum efficiency coefficient (α_{cx} , mol mol⁻¹) and a conversion factor converting carbohydrates into dry matter. Further constraints on assimilation are then applied by dimensionless environmental factors varying between 0 and 1 (1 indicates optimal conditions). These factors, also referred to as modifiers, are multiplicative and represent the influence of vapour pressure deficit (D) or soil moisture, which ever is most limiting, mean air temperature (T), frost, and soil nutrition on photosynthetic assimilation (Sands 2004). Gross primary productivity (P_g , t ha⁻¹ d⁻¹) is then converted to net primary productivity (P_n , t ha⁻¹ d⁻¹) using a simple P_n / P_g ratio (Y).

2.2 Biomass allocation and mortality

P_n is then allocated to the different plant components (roots, foliage and stems including branches) at each time step. Allocation to roots is proportional to the harshness of the environment. It is influenced by site fertility, stand age and the most limiting between D or soil water, but does not fall below or exceed set values of minimum and maximum allocation to roots. The remaining P_n is shared between stems and foliage through a foliage-to-stem allocation ratio, given by an allometric relationship with mean diameter at breast height (Sands & Landsberg 2002, Sands 2004). DBH is itself obtained from an allometric relationship with stem biomass. Whereas P_n partitioning parameters must generally be estimated from fitting methods, those pertaining to the allometric relationship between stem biomass and diameter can be derived from forest mensuration (Sands & Landsberg 2002). Mortality is applied

1
2
3
4 124 through the self thinning 3/2 law, which sets an upper limit to the mean single-tree
5
6 125 stem mass at a given stocking level.

126 **2.3 Soil water balance**

127 Available soil water θ (mm month⁻¹) is governed by rainfall interception by the
128 canopy (i_R), rainfall (R_P , mm month⁻¹) and evapotranspiration (E_T , mm month⁻¹). If the
129 maximum available water at saturation is exceeded, the excess of water is lost as
130 runoff.

$$131 \quad \theta = (1 - i_R)R_P - E_T \quad [1]$$

132 Rainfall interception increases with canopy LAI and is taken as a fraction of rainfall.
133 E_T is calculated using the Penman Monteith equation controlled by the canopy
134 conductance, solar radiation and D . Canopy conductance (g_C , m s⁻¹) increases with
135 LAI but is bounded by the LAI value at which conductance is at a maximum (g_{C_x} , m s⁻¹).
136 The relationship between g_C and LAI is further controlled by age and the most
137 limiting factor controlling stomatal aperture, either vapor pressure deficit or soil
138 moisture. Further details on 3-PG can be found in Landsberg and Waring (1997) and
139 Sands and Landsberg (2002).

140 **3 Materials and methods**

141 **3.1 Study site and available datasets**

142
143 The calibration of the 3-PG model was conducted for Corsican Pine stands of yield
144 class 14 using existing data from a 20,000 ha forest plantation, East Anglia, UK
145 (Thetford forest, 52°30' N, 0°30' E). The stands in Thetford are assumed under an
146 intermediate spacing, intermediate thinning and 80 years rotation regime (Edwards &
147 Christie 1981).

148 3.2 Field based datasets

149 The following datasets were used in the calibration: (i) the UK Forestry Commission
150 GIS database, a spatially exhaustive catalogue comprising of approximate stand level
151 information on species, yield class, planting year, planting density and stemwood
152 volume (ii) the Maestro-1 1989 campaign and the 2000 SHAC campaign datasets
153 (Baker 1992, Baker et al. 1994, Skinner and Luckman, 2000) which consist of ground
154 data collected on stand level information (each sampled stand was allocated a
155 Forestry Commission code maintaining consistency with the GIS database) and (iii)
156 datasets collected in Thetford over the years (e.g. Ovington 1957, Corbett 1973,
157 Roberts 1976, Beadle et al. 1982, Beadle et al. 1985a, Beadle et al. 1985b, Beadle et
158 al. 1985c, Stewart 1988, Mencuccini & Grace 1996).

160 The model was initialised for a stand aged 15 years using chronosequenced biomass
161 data obtained from the Maestro dataset (Baker 1992, Baker et al. 1994). Initialising
162 the model at this age removes the need for extra parameterisation required by early
163 growth processes while still enabling the calibration of key parameters. Root, stem
164 and foliage biomass were 7.1 t/ha, 22 t/ha and 9.8 t/ha respectively. Initial stocking of
165 3955 trees per hectare was obtained from the production tables (Edwards and Christie
166 1981).

168 The required climatic data were derived from the Climate Research Unit datasets and
169 the Cambridge botanical garden meteorological station (New et al. 2000,
170 <http://badc.nerc.ac.uk/home/index.html>). The area is characterised by a relatively flat
171 topography and insignificant climatic variations within the site were assumed
172 (Ovington 1957). Long term average climatic conditions are summarized in Table 1.

Table 1

Other input variables include site latitude, an estimate of soil fertility and texture, as well as available soil water (mm per depth of rooting zone, in meters). The soils of the plantation are of poor quality, predominantly sandy with deep alkaline chalky bedrock and drain freely throughout the forest (Corbett 1973, Mencuccini & Grace 1996). Minimum available water was estimated based on field measurements taken during the drought year of 1976. During the drought, measurements have shown that at least 170mm soil water was available (Roberts et al. 1982). The maximum available water was assumed as 250mm based on: (a) the assumption that storage capacity for sandy soils is approximately 150mm per metre of soil with a permanent wilting point of 50 mm and (b) field measurements taken in Thetford, showing that 95% of roots are located in the first meter of soil (Roberts 1976). Given the documented deep bedrock (Corbett 1973), we assumed a 2 meters soil layer.

All runs were made with 3-PGpjs, a Visual Basic implementation of 3-PG in Excel available at http://www.ffp.csiro.au/fap/3pg/download_details.htm.

3.3. Remote sensing datasets and processing

SAR, Hyperspectral, and LiDAR datasets acquired in 2000 were included in the calibration. These datasets were used instead of alternative empirical, approximate yield based tables given their site specific nature and our ability to quantify variability in the estimates of biophysical variables.

3.3.1 SAR

A multi-frequency, Synthetic Aperture Radar instrument (E-SAR) was flown on the 31st May 2000 in wide swath mode, with data collected at L-HH, L-HV, L-VV, X-

1
2
3 199 VV, plus repeat-pass L-band fully polarimetric data. The mean stand backscatter
4
5 200 coefficient, σ^0 (dB), and the mean stand interferometric coherence were calculated for
6
7 201 the L-HH, L-VV and L-HV polarisations from the geocoded E-SAR data. Although
8
9 202 InSAR data were available, only the interferometric coherence and backscatter were
10
11 203 used for the work described here. A neural network was trained to estimate stand top
12
13 204 height in Corsican Pine stands from the E-SAR backscatter and coherence data. The
14
15 205 data were divided in half, with half used as a training data set to train the neural
16
17 206 network and the other half used as a testing data set, to assess the ability of the
18
19 207 proposed relationships against unseen data. The inputs to the network were the three
20
21 208 mean stand values for coherence (L-HH, L-HV, L-VV) plus the three mean stand
22
23 209 values for backscatter (L-HH, L-HV, L-VV). The neural network was a 1-hidden
24
25 210 layer network trained with a Levenberg-Marquardt based learning algorithm. Two
26
27 211 network structures were investigated, with 2 and 11 nodes in the hidden layer,
28
29 212 respectively. To ensure that the best network was selected, 50 trained networks were
30
31 213 generated, with the best network selected based on minimum RMSE against the test
32
33 214 data set. The lowest error was produced by a network with two nodes in the hidden
34
35 215 layer resulting in a R^2 of 0.90 and a RMSE of 2.51m when tested against the test data
36
37 216 set (Rowland et al. 2003).
38
39
40
41
42
43
44

45 217 *3.3.2 Hyperspectral*

46
47 218 Hyperspectral data was acquired using the SHAC HyMAP imaging spectrometer in
48
49 219 June 2000 (126 contiguous bands, 436-2486 nm at 15 nm spectral resolution, 4m
50
51 220 spatial resolution). Atmospheric correction was applied by DLR and the overlapping
52
53 221 scenes were georectified, mosaicked and normalised to minimise the effect of sensor
54
55 222 look angle. Signal to noise ratio analysis was conducted to remove noisy atmospheric
56
57 223 water absorption bands from the original dataset.
58
59
60

224 3.3.3 LiDAR

225 E-SAR and hyperspectral datasets were complemented in June 2000 with first and last
226 return data acquired by means of a small footprint Airborne Laser Terrain Mapper
227 (Optech ALTM 1210). The ALTM emits laser pulses at a wavelength of 1047nm
228 (NIR) where vegetation is highly reflective. The data was collected at footprint size of
229 0.05m^2 . A $\pm 10^\circ$ scanning orientation perpendicular to the flight path was selected
230 which generated irregular ground measurements ranging between 2.80m^2 to 6.50m^2 .
231 The precision of the instrument was estimated at 0.60m in the x and y position and
232 0.15 m in z (www.optech.on.ca).

233 A digital canopy height model (DCHM) was obtained by subtraction of a digital
234 terrain model (DTM) from a digital surface model (DSM). The DSM and the DTM
235 were derived from the first and last significant LiDAR returns respectively
236 (methodology described in Gaveau and Hill 2003, Patenaude et al. 2004 and Rowland
237 et al. 2003). Both the first and last return were converted from a point to a gridded
238 format. The DTM was then produced by applying a minimum value filter to identify
239 local height minima in the gridded LiDAR last return product. Top height per stand
240 was extracted from the DCHM based on the maximum canopy height per stand
241 ($R^2=0.94$, RMSE 1.68m, bias 0.48m). The use of percentiles was also tested (90^{th} ,
242 95^{th} , 97.5^{th} and 99^{th}). However, whilst they may be appropriate for mean stand height,
243 they were found to underestimate canopy top height for the Thetford stands (Rowland
244 et al. 2003).

245

246 4 Bayesian calibration

247 In Bayesian statistics, probability is interpreted as the degree of certainty for some
248 quantity, conditional to available data and knowledge. As model parameter values are

1
2
3
4 249 not precisely known, this uncertainty can be represented as a probability distribution
5
6 250 over the parameters. Thus, if we define θ as a parameter vector for 3-PG, then $P(\theta)$
7
8 251 represents its probability distribution and $P(f(\theta))$ the uncertainty in model outputs
9
10 252 ($f(\theta)$) generated by the uncertainty in the parameters. In this context, Bayesian
11
12 253 calibration is a method enabling $P(\theta)$ to be updated as new data come in (e.g. Figure
13
14
15 254 1).

18 255 **Figure 1**

19 256
20 257 Given a dataset D , we can derive $P(\theta|D)$ from $P(\theta)$ by applying Bayes Theorem:

$$21 258 P(\theta|D) = P(\theta) P(D|\theta) / P(D) \quad [2]$$

22
23
24
25 259 In Bayesian terminology and as illustrated in Figure 1, $P(\theta|D)$ is the updated or
26
27 260 posterior parameter distribution; $P(\theta)$ is the original distribution, referred to as the
28
29 261 prior; $P(D|\theta)$ is the conditional probability of the data for a given parameterisation,
30
31 262 called the likelihood; and $P(D)$ is a normalization constant that may be referred to as
32
33 263 the evidence.
34
35
36
37
38
39

40 265 **4.1 The prior**

41 266 The prior distribution is built from marginal distributions, which reflect our current
42
43 267 knowledge of parameters and outputs. The distribution that best describes the
44
45 268 available information about parameters must be used. When limited information is
46
47 269 available, Van Oijen *et al.* (2005) suggest the use of uniform distributions, bounded
48
49 270 by a biophysically or biologically reasonable maximum and minimum value for each
50
51 271 parameter. Table 2 presents values to 3-PG parameters and the prior distribution
52
53 272 selected for calibration.
54
55
56
57
58

59 273 **Table 2**

1
2
3 274 The prior distributions were set uniform, bounded by a maximum and minimum value
4
5 275 for each parameter. Boundaries to the prior were obtained from direct observation on
6
7
8 276 Corsican pine stands in Thetford (CP-T), from literature on Corsican or other pine
9
10 277 species (P-L), from surrogate species or 3-PG set default values (D) or finally as best
11
12
13 278 guess estimates or fitting approaches (F) (Table 2). Key parameters difficult to
14
15 279 measure in the field and for which little information was available were included in
16
17
18 280 the calibration. The remaining parameters were prescribed constant values (Table 2),
19
20 281 including the parameters pertaining to the allometric relationship between stem mass
21
22 282 and diameter at breast height (a_S and n_S).
23
24
25
26

27 284 **4.2 The likelihood**

285 A total of 28 data points were used in the calibration exercise: LiDAR derived heights
286 (4); E-SAR and field based estimates of total above-ground biomass (4 and 1
287 respectively); field based estimates of stem, foliage and root biomass (3, 3 and 5
288 respectively); and Hyperspectral and ground based LAI estimates (7 and 1
289 respectively).

290 *4.2.1 LiDAR heights*

291 LiDAR heights were taken as surrogates of top heights (section 3.3.3). These were
292 aggregated and averaged per 15 years age classes (Figure 2). Uncertainty was
293 estimated as standard deviations to height averages per class. An additional ± 0.5 m
294 error was added to small samples ($n < 9$).

295 *4.2.2 E-SAR and field based above-ground biomass*

296 Above-ground biomass data were derived from E-SAR top height estimates.
297 Conversion of top height to above ground biomass involved two stages of calculations
298 (Rowland et al. 2003, summarised here): (i) conversion of top height to stemwood

299 volume using an empirical relationship derived from Edwards & Christie (1981) (ii)
 300 conversion of stemwood volume to biomass using a biomass expansion factor and a
 301 generic basic density coefficient (1.5 for temperate pine species, Milne 1992, IPCC
 302 2004; 0.43 t m⁻³, Hamilton 1975, respectively). E-SAR biomass estimates were
 303 plotted against yield table estimates (log transformed, Figure 2). Untransformed
 304 standard deviations of biomass (aggregated and averaged per 15 years age classes)
 305 were used as error estimates. An additional ±10 t ha⁻¹ uncertainty was added to small
 306 samples (n<9).

307 **Figure 2**

308 *4.2.3 Stem, foliage and root biomass*

309 Stem and foliage biomass data points were derived from Baker (1992) and Baker et al.
 310 (1994). For root biomass, a root to shoot ratio was derived from destructive
 311 measurements made in 6 mature Scot pine stands (Ovington, 1957). The ratio below
 312 to above-ground across ages (0.3, Std 0.05) was assumed representative to that of
 313 Corsican pine. This value is also consistent with that given by the IPCC (2003) for
 314 temperate coniferous forests. Five root biomass points were derived. A ±10% relative
 315 error was assumed.

316 *4.2.4 LAI*

317 Given the absence of ground based or alternative sources, LAI data points were
 318 derived from hyperspectral data. LAI in pine plantations generally exhibit a growth
 319 pattern expressed as (e.g. Mencuccini and Grace 1996):

$$320 \quad LAI = ae^{-0.5\left(\frac{\ln(x/x_0)}{b}\right)^2} \quad [3]$$

321 Where a represents the maximum LAI reached by a stand, x_0 the age at which this
 322 maximum is reached and b , a parameter controlling the tailing off of the LAI curve.

323 Equation 3 was solved in a three way procedure: (i) Corsican pine stands in the GIS

324 database were co-registered to the image allowing the chronosequencing of leaf area
 325 index (LAI) throughout the rotation (ii) based on the results by Lee et al. (2004) and
 326 Pu and Gong (2004) where close proportionality was found between LAI and the
 327 primary axis of a principal component analysis (PCA) for the different wavelengths,
 328 PCA was used to estimate LAI growth patterns in Thetford CP stands. Averaged
 329 values per stand were plotted against stand age using the GIS attribute database. The
 330 x_0 and b parameters, which pertain to the shape of the curve only, not the magnitude
 331 of LAI were solved by minimising the distance between chronological PCA points
 332 and the Equation 3 (Figure 3). (iii) Conversion of PCA values to LAI, was completed
 333 using the available projected LAI datum (Ovington, 1957). Large relative
 334 uncertainties (30%) were assumed.

335 **Figure 3**

336 *4.2.4 Estimating the likelihood*

337 To calculate the likelihood, i.e. the probability of the data given a model
 338 parameterisation $P(D|\theta)$, information about measurement error must be available.
 339 Assuming that the errors associated with our data are independent and Gaussian,
 340 $P(D|\theta)$ then follows from the comparison of each data point D_i with the corresponding
 341 model output $f_i(\theta)$ as:

$$342 \quad P(D|\theta) = \prod_i^n \varphi(D_i - f_i(\theta); 0, SD_i) \quad [4]$$

343 where, φ symbolizes a Gaussian function with 0 and SD_i as mean and standard
 344 deviation of errors, and $n=28$, the number of points in the data sample.

346 **4.3 The posterior: a Monte Carlo estimation of the posterior distribution**

347 The application of Bayes Theorem to process-based models has traditionally been
 348 hampered by two problems: (i) the models cannot be solved analytically, so a

1
2
3
4 349 sampling method to explore the parameter space is required (we define parameter
5
6 350 space as the space entailing all combinations of possible parameter vectors defined by
7
8 351 the prior) (ii) the models need to be run at every sampled point in parameter space (to
9
10 352 calculate the probability), a highly time consuming and computer intensive process. In
11
12 353 recent years, Markov Chain Monte Carlo (MCMC) methods have been found useful
13
14 354 to resolve this type of problem (Van Oijen et al. 2005). Here, we used the MCMC
15
16 355 Metropolis Hastings Random Walk, which has the two following steps:
17
18
19
20 356

21
22 357 1. After randomly choosing a first parameter vector, propose a new candidate for the
23
24 358 next parameter vector in the chain from the parameter space as:

$$25 \quad 26 \quad 27 \quad 28 \quad 29 \quad 30 \quad 31 \quad 32 \quad 33 \quad 34 \quad 35 \quad 36 \quad 37 \quad 38 \quad 39 \quad 40 \quad 41 \quad 42 \quad 43 \quad 44 \quad 45 \quad 46 \quad 47 \quad 48 \quad 49 \quad 50 \quad 51 \quad 52 \quad 53 \quad 54 \quad 55 \quad 56 \quad 57 \quad 58 \quad 59 \quad 60$$

$$359 \quad \theta' = \theta_t + \varepsilon \quad [5]$$

360 Where θ' is the proposed candidate, θ_t is the current parameter vector and ε is a
361 random vector enabling the exploration of the parameter space. ε is selected from a
362 Gaussian distribution with mean 0. Its standard deviation should be chosen to enable a
363 wide exploration of the parameter space and to yield acceptance rates (of the rule
364 described below) between 20 and 50%. We found that a standard deviation of 0.05
365 gave good results.

366 2. Run the model with the proposed candidate. The rule for accepting or rejecting the
367 candidate has two components, namely:

368 (i). Calculate the ratio of probabilities β , which cancels out the need for estimating
369 $p(D)$:

$$370 \quad \beta = \frac{p(\theta' | D)}{p(\theta_t | D)} = \frac{p(D | \theta')p(\theta')}{p(D | \theta_t)p(\theta_t)} \quad [6]$$

371 (ii). Generate a uniform random variable u ($0 \leq u \leq 1$). The new candidate θ' is accepted
372 and becomes θ_{t+1} if $u \leq \beta$. If $\beta \geq 1$, the proposal is always accepted.

373 The acceptance criterion, based on the selection of a random variable, thus enables the
374 acceptance of marginal θ_i with probability lower than their predecessor in the chain.

375 This procedure contrasts with many optimisation approaches by allowing downhill
376 steps. The ratio of probabilities, β , also implies that the number of data points used in
377 the calibration has no weight on the selection of a parameter vector (the use of 5 LAI
378 data points instead of 100 has no influence). The weight is given by the data and
379 parameters' uncertainty.

380

381 Because the posterior distribution cannot be described analytically, the results are
382 presented in the form of marginal distributions using descriptive statistics. As
383 suggested by Van Oijen et al. (2005), in addition to means and standard deviations,
384 we present the maximum *a posteriori* (MAP) estimate of θ , considered as the single
385 "best" parameter value estimated from the MCMC sample.

$$386 \theta_{MAPx} = \arg \max_{\theta} p(\theta | D) \quad [7]$$

387 Although this should not be interpreted as an optimised parameter vector, this
388 nevertheless provides information as to what vector has the highest probability density
389 given the available data.

390

391 **4.4 Sensitivity analysis**

392 The sensitivity of a given model output with respect to a parameter (and vice versa)
393 has also been estimated from partial correlations calculated between the 25 000
394 parameter and output vectors. This resulted in a 14x28 partial correlation matrix.

395

396 **5 Results and discussion**

397

1
2
3
4 398 A 25 000 vectors sample was generated from the posterior distribution using the
5
6 399 MCMC sampling approach. Figure 4 shows an example of MCMC trace plot and the
7
8 400 resulting marginal posterior distribution for the fertility rating (*FR*) parameter.
9

10
11 **Figure 4**

12 402 Summary statistics to the marginal distributions of parameters are presented in Table
13
14 403 3, which include the mean and standard deviation and the vector of highest *a*
15
16 404 *posteriori* probability density (θ_{MAP}). Figure 5 shows the mean model outputs from the
17
18 405 25,000 estimates, the 3-PG outputs from θ_{MAP} (best fit) and the datasets used in the
19
20 406 likelihood.
21
22
23

24
25 **Table 3**

26
27 **Figure 5**

28 409
29 410 Partial correlations between parameters and outputs are presented in Figure 6. These
30
31 411 are illustrated under the form of a colour fingerprint between the 14 calibrated
32
33 412 parameters and the 28 model outputs. High negative correlations are shown as dark
34
35 413 blue and high positive correlations, as dark red. Light regions indicate weak or no
36
37 414 correlation.
38
39

40
41 **Figure 6**

42
43 416
44 417
45 418 In Table 3, one can observe the close similarity between the θ_{MAP} vector and the
46
47 419 posterior mean $\overline{\theta(i)}$, suggesting that both vectors converge towards a single solution
48
49 420 (a local maximum within the full posterior distribution). Corresponding model
50
51 421 outputs are shown in Figure 5. Outputs from θ_{MAP} (best fit) and $\overline{\theta(i)}$ (posterior mean)
52
53 422 also lie closely to data error bounds. Note the smaller error bounds to the posterior in
54
55 423 comparison with the data. While above ground, stem and foliage biomass model
56
57 424 dynamics closely match those observed on the ground, allocation to roots appears to
58
59
60

1
2
3
4 425 level towards 25 years into the rotation and decrease thereafter. This appears to be an
5
6 426 artefact of the model structure, rather than parameterisation. Additional MCMC
7
8 427 analysis was conducted (results not shown here) to explore the influence of the model
9
10 428 structure on the model outputs. The data used in the calibration were given here
11
12
13 429 extremely high standard deviations, such that the distributions tended towards
14
15 430 uniform. Likewise, large but realistic ranges of parameter values (with uniform
16
17 431 distributions) were given. In doing so, the data became uninformative and the
18
19
20 432 observed dynamics in the model outputs resulted predominantly from the model
21
22 433 structure therefore representing “a typical behaviour” and dynamic of the model. In
23
24 434 average, the model will tend to produce certain results, unless specific
25
26
27 435 parameterisation is provided. The results showed that in average, 3-PG simulates
28
29 436 above-ground growth in an increasing, near linear fashion; LAI follows an
30
31 437 exponential increase along the rotation without tail off; and root allocation increases
32
33 438 early in the rotation but decreases thereafter (in a similar dynamic as that observed in
34
35 439 Figure 5). This suggests that comparatively to above ground biomass and LAI, whose
36
37 440 dynamics are sensitive to parameterisation, root biomass is predominantly determined
38
39 441 by the model structure. In the Bayesian calibration conducted here, even when data
40
41 442 with small uncertainties are used, the underlying influence of the model structure is
42
43 443 evident.
44
45
46
47
48
49
50
51
52
53
54
55
56
57
58
59
60

444
445 Careful examination of Figure 6 also provides strong insights into the multivariate
446 interactions imbedded in the model. For instance, one can observe consistent
447 correlation throughout the rotation between parameters and specific outputs. The
448 optimum temperature for growth, T_{opt} is consistently negatively correlated with all
449 model outputs considered. As T_{opt} increases, productivity is reduced. Most probable

1
2
3
4 450 T_{opt} values (θ_{MAP} and $\overline{\theta(i)} \approx 20^\circ \text{C}$) are reasonable. The species is endemic to elevated
5
6 451 altitude Mediterranean regions where hot days are four times more frequent than in
7
8 452 Lowland Britain (Brown 1960, Kerr 2000). However, the stands in Thetford seldom
9
10 453 grow under optimal temperature where annually, the average temperature is
11
12 454 approximately 10°C . Similarly, as the maximum canopy quantum efficiency
13
14 455 increases (α_{Cx}), a consistent increase in all biomass outputs is observed. An expected
15
16 456 result, as the net primary production is proportional to the product of the maximum
17
18 457 canopy quantum efficiency (α_{Cx}), the P_n / P_g ratio (Y), light interception and
19
20 458 environmental constraints. Other consistent correlations are found between specific
21
22 459 leaf area (σ_l), litterfall rate (γ_{Fl}), the ratio of foliage to stem partitioning at maturity
23
24 460 (p_{20}) and LAI; between the fertility rating (FR) and above ground components
25
26 461 (biomass and LAI); or root turnover (γ_R) and root biomass. As for decreasing or
27
28 462 increasing correlations with outputs throughout the rotation, these can provide
29
30 463 indications as to where the influence of a parameter is most significant. With
31
32 464 Bayesian calibration, the inverse is also true: data collected at specific moments
33
34 465 during the rotation may be particularly useful in calibrating and reducing the
35
36 466 uncertainty for a given parameter. For instance, maximum stand age (t_x) plays an
37
38 467 important role late in the rotation, as it controls productivity reduction as stand ages.
39
40 468
41
42 469 The results presented above serve three purposes. Firstly, they present a first attempt
43
44 470 to parameterise 3-PG for Corsican pine stands. While occupying more than 30
45
46 471 thousand hectares of the UK territory (Forestry Commission, 2001), relatively limited
47
48 472 information is available on Corsican pines, comparatively to more economically
49
50 473 viable species such as Sitka spruce and Scots pine. Thetford forest, one of the largest
51
52 474 UK plantations, served as a case study. Model outputs from parameterisation with (i)

1
2
3
4 475 θ_{MAP} (parameter vector with highest probability density given available data), and (ii)
5
6 476 the mean from the marginal distributions were presented. Secondly, we illustrated the
7
8 477 ability of Bayesian calibration as a framework to integrate remote sensing datasets,
9
10 478 often the only source of data available at the spatial and temporal scales required, into
11
12 479 ecological modelling. This approach enables uncertainty analysis despite the fact that
13
14 480 limited data (and often of poor quality), is available. With Bayesian calibration, given
15
16 481 relatively diffuse priors (e.g. uniform distributions), the posteriors will be at first
17
18 482 strongly influenced by the data. This influence however decreases as new data come
19
20 483 in and as the uncertainty in the prior decreases. Thirdly, despite the fact that the
21
22 484 probability density of a scalar model output or parameter is nearly nil, process based
23
24 485 models used in forestry are commonly parameterised by adjusting the value of
25
26 486 selected parameters for the model output to fit the data time series, without any
27
28 487 indication of parameter and output uncertainties. The parameterisation of 3-PG for
29
30 488 novel species is unfortunately no exception (e.g. White *et al.* 2000, Sands and
31
32 489 Landsberg 2002, Sands 2004, Stape *et al.* 2004 and Almeida *et al.* 2004). The results
33
34 490 presented here have shown that given ever increasing computing power and speed,
35
36 491 uncertainty quantification and model parameterisation can be achieved with relative
37
38 492 ease using Bayesian calibration.
39
40
41
42
43
44
45
46
47
48

49 494 **6 Conclusion**

50
51 495 While both optimisation and Bayesian approaches address the need to test whether a
52
53 496 model can predict available data or not, in optimisation, parameter values are adjusted
54
55 497 such that the model yields outputs closest to the data. This precludes the integration of
56
57 498 uncertain datasets, ancillary or remotely sensed, which can provide information on
58
59 499 variables not currently or commonly compiled. Additionally, approaches such as the
60

1
2
3 500 maximum-likelihood do not enable the full exploration of the parameter landscape.
4
5
6 501 The resulting parameter vector may therefore only be from a local maximum.
7
8 502 Conversely, Bayesian calibration advocates the quantification of uncertainties to
9
10 503 parameters, thereby yielding uncertainties in model outputs, over the derivation of an
11
12 504 optimised set of parameter based on a goodness-of-fit approach (e.g. the maximum-
13
14 505 likelihood approach). By doing so, Bayesian calibration provides a means to conduct
15
16 506 truly integrative work for quantifying model output and parameter uncertainty, while
17
18 507 considering all the existing information, including that enclosed in the model itself.
19
20
21
22
23
24

25 **Acknowledgements**

26
27 510 The authors would like to thank Maurizio Mencuccini (University of Edinburgh),
28
29 511 David Cameron (CEH Edinburgh), Richard Waring (Oregon State University), and
30
31 512 Peter Savill (University of Oxford) for sharing data and advices. Thanks are due to the
32
33 513 British Atmospheric Data Centre and the Forestry Commission for providing access to
34
35 514 databases, to the Environment Agency for making available the LiDAR data, and to
36
37 515 all those involved in the Thetford fieldwork campaigns in 1989 and 2000. The E-SAR
38
39 516 data were acquired during the SHAC 2000 campaign by Natural Environmental
40
41 517 Research Council and the British National Space Centre.
42
43
44
45
46
47
48
49

50 **References**

51
52
53 521 Almeida A.C., Landsberg J.J., Sands P.J. (2004) Parameterisation of 3-PG model for
54
55 522 fast-growing Eucalyptus grandis plantations. *Forest Ecology and Management*
56
57 523 193:179-195
58
59
60 524

- 1
2
3 525 Baker J.R. (1992) The UK element of the Maestro-1 SAR campaign. *International*
4
5
6 526 *Journal of Remote Sensing* 13:1593-1608
7
8 527
9
10 528 Battaglia M., Sands P.J. (1998) Process-based forest productivity models and their
11
12 529 application in forest management. *Forest Ecology and Management* 102:13-32
13
14 530
15
16
17 531 Baulies, X. and Pons, X. (1995). Approach to forestry inventory and mapping by
18
19 532 means of multispectral airborne data. *International Journal of Remote Sensing*,
20
21 533 16:61-80.
22
23 534
24
25
26
27 535 Beadle C.L., Jarvis P.G., Talbot H., Neilson R.E. (1985a) Stomatal Conductance and
28
29 536 Photosynthesis in a Mature Scots Pine Forest .2. Dependence on
30
31 537 Environmental Variables of Single Shoots. *Journal of Applied Ecology*
32
33 538 22:573-586
34
35
36 539
37
38
39 540 Beadle C.L., Neilson R.E., Talbot H., Jarvis P.G. (1985b) Stomatal Conductance and
40
41 541 Photosynthesis in a Mature Scots Pine Forest .1. Diurnal, Seasonal and Spatial
42
43 542 Variation in Shoots. *Journal of Applied Ecology* 22:557-571
44
45
46 543
47
48 544 Beadle C.L., Talbot H., Jarvis P.G. (1982) Canopy Structure and Leaf-Area Index in a
49
50 545 Mature Scots Pine Forest. *Forestry* 55:105-123
51
52 546
53
54
55 547 Beadle C.L., Talbot H., Neilson R.E., Jarvis PG (1985c) Stomatal Conductance and
56
57 548 Photosynthesis in a Mature Scots Pine Forest .3. Variation in Canopy
58
59
60

- 1
2
3 549 Conductance and Canopy Photosynthesis. *Journal of Applied Ecology* 22:587-
4
5 550 595
6
7
8 551 Brown, J.M.B. (1960). The Corsican pine in its native island, Part 2. *Empire Forestry*
9
10 552 *Review* 39: 422-436.
11
12 553 Coops N.C., Waring R.H. (2001) The use of multiscale remote sensing imagery to
13
14 derive regional estimates of forest growth capacity using 3-PGS. *Remote*
15 554
16 *Sensing of Environment* 75 (3): 324-334
17 555
18
19
20 556
21
22 557 Coops N.C., Waring R.H., Landsberg J.J. (2001) Estimation of potential forest
23
24 productivity across the Oregon transect using satellite data and monthly
25 558
26 weather records. *International Journal of Remote Sensing* 22:3797-3812
27 559
28
29 560
30
31 561 Corbett W.M. (1973) Breckland forest soils: special survey no.7, Rothamsted
32
33 Experimental Station, Harpenden, Herts
34 562
35
36 563
37
38 564 Cousens J.E. (1988) Report of a 12-Year Study of Litter Fall and Productivity in a
39
40 Stand of Mature Scots Pine. *Forestry* 61:255-266
41 565
42
43 566
44
45 567 Cramer W., Field C.B. (eds) (1999) The Potsdam NPP model intercomparison, *Global*
46
47 *Change Biology Vol 5*. Blackwell Science, Oxford.
48 568
49
50 569
51
52 570 Edwards P.N., Christie J.M. (1981) Yield models for forest management, *Forestry*
53
54 *Commission booklet ; no. 48* HMSO, London, 274 p.
55 571
56
57 572
58
59
60

- 1
2
3 573 Esprey L.J., Sands P.J., Smith C.W. (2004) Understanding 3-PG using a sensitivity
4
5
6 574 analysis. *Forest Ecology and Management* 193:235-250
7
8 575
9
10 576 Ewel K.C., Gholz H.L. (1991) A Simulation-Model of the Role of Belowground
11
12 577 Dynamics in a Florida Pine Plantation. *Forest Science* 37:397-438
13
14 578
15
16
17 579 Flower-Ellis J.G.K., Olsson L. (1993) Estimation of volume, total and projected area
18
19 580 of Scots pine needles from their regression on length. *Studia Forestalia*
20
21 581 *Suecica* 190:1-19
22
23
24 582
25
26
27 583 Forestry Commission (2001) National inventory of woodlands and trees. Report No.
28
29 584 <http://www.forestry.gov.uk/forestry/HCOU-54PG9U>, Forest Research,
30
31 585 Forestry Commission, Edinburgh
32
33 586
34
35
36 587 Gash J.H.C., Shuttleworth W.J., Lloyd C.R., Andre J.C., Goutorbe J.P., Gelpe J.
37
38 588 (1989) Micrometeorological Measurements in Les-Landes Forest During
39
40 589 Hapex-Mobilhy. *Agricultural and Forest Meteorology* 46:131-147
41
42 590
43
44
45
46 591 Gertner G.Z., Fang S.F., Skovsgaard J.P. (1999) A Bayesian approach for estimating
47
48 592 the parameters of a forest process model based on long-term growth data.
49
50 593 *Ecological Modelling* 119:249-265
51
52 594
53
54
55 595 Ghazoul J., McAllister M. (2003) Communicating complexity and uncertainty in
56
57 596 decision making contexts: Bayesian approaches to forest research.
58
59 597 *International Forestry Review* 5:9-19
60

1
2
3
4
5
6
7
8
9
10
11
12
13
14
15
16
17
18
19
20
21
22
23
24
25
26
27
28
29
30
31
32
33
34
35
36
37
38
39
40
41
42
43
44
45
46
47
48
49
50
51
52
53
54
55
56
57
58
59
60

598

599 Gill R.A., Jackson R.B. (2000) Global patterns of root turnover for terrestrial
600 ecosystems. *New Phytologist* 147:13-31

601

602 Granier A., Biron P., Breda N., Pontailleur J.Y., Saugier B. (1996) Transpiration of
603 trees and forest stands: Short and longterm monitoring using sapflow methods.
604 *Global Change Biology* 2:265-274

605

606 Green E.J., MacFarlane D.W., Valentine H.T. (2000) Bayesian synthesis for
607 quantifying uncertainty in predictions from process models. *Tree Physiology*
608 20:415-419

609

610 Green E.J., MacFarlane D.W., Valentine H.T., Strawderman W.E. (1999) Assessing
611 uncertainty in a stand growth model by Bayesian synthesis. *Forest Science*
612 45:528-538

613

614 Hamilton G.J. (1975) Forest mensuration handbook, *Forestry Commission booklet no.*
615 39 HMSO, London, 274 p.

616

617 Hyypä J., Hyypä H., Inkinen M., Schardt M., Ziegler M. (2000). Forest inventory
618 based on laser scanning and aerial photography. *Laser Radar Technology and*
619 *Applications*, V:106-118.

620

621 Hyypä, J., Kelle, O., Lehikoinen, M., Inkinen, M. A (2001). segmentation-based
622 method to retrieve stem volume estimates from 3-D tree height models

- 1
2
3
4 623 produced by laser scanners. *IEEE Transactions on Geoscience and Remote*
5
6 624 *Sensing*, 39 (5): 969-975.
7
8 625
9
10 626 Jansen M.J.W. (1999) Data use and Bayesian statistics for model calibration. In: Stein
11
12 627 A., Penning de Vries F.W.T. (eds) *Data and models in action*. Kluwer,
13
14 628 Dordrecht, p 69-80
15
16
17 629
18
19 630 Kelliher F.M., Leuning R., Raupach M.R., Schulze E.D. (1995) Maximum
20
21 631 Conductances for Evaporation from Global Vegetation Types. *Agricultural*
22
23 632 *and Forest Meteorology* 73:1-16
24
25
26 633
27
28 634 Kelliher F.M., Leuning R., Schulze E.D. (1993) Evaporation and Canopy
29
30 635 Characteristics of Coniferous Forests and Grasslands. *Oecologia* 95:153-163
31
32
33 636
34
35 637 Kerr, G. (2000). Natural regeneration of Corsican pine (*Pinus nigra* subsp *laricio*) in
36
37 638 Great Britain. *Forestry* 73(5): 479-488.
38
39
40 639
41
42 640 Landsberg J.J., Waring R.H. (1997) A generalised model of forest productivity using
43
44 641 simplified concepts of radiation-use efficiency, carbon balance and
45
46 642 partitioning. *Forest Ecology and Management* 95:209-228
47
48
49 643
50
51 644 Law B.E., Waring R.H., Anthoni P.M., Aber J.D. (2000) Measurements of gross and
52
53 645 net ecosystem productivity and water vapour exchange of a *Pinus ponderosa*
54
55 646 ecosystem, and an evaluation of two generalized models. *Global Change*
56
57 647 *Biology* 6:155-168
58
59
60

- 1
2
3 648
4
5
6 649 Levy P.E., Hale S.E., Nicoll B.C. (2004) Biomass expansion factors and root : shoot
7
8 650 ratios for coniferous tree species in Great Britain. *Forestry* 77:421-430
9
10 651
11
12 652 Luckman A., Baker J., Kuplich T.M., Yanasse C.D.F., Frery A.C. (1997) A study of
13
14 653 the relationship between radar backscatter and regenerating tropical forest
15
16 654 biomass for spaceborne SAR instruments. *Remote Sensing of Environment*
17
18 655 60:1-13
19
20
21
22 656
23
24 657 Mencuccini M., Grace J. (1996) Hydraulic conductance, light interception and needle
25
26 658 nutrient concentration in Scots pine stands and their relations with net primary
27
28 659 productivity. *Tree Physiology* 16:459-468
29
30
31
32 660
33
34 661 New M., Hulme M. and Jones P. (2000) Representing twentieth-century space-time
35
36 662 climate variability. Part II: Development of 1901-96 monthly grids of
37
38 663 terrestrial surface climate. *Journal of Climate* 13(13):2217-2238
39
40 664 http://www.cru.uea.ac.uk/~markn/cru05/cru05_intro.html
41
42 665
43
44 666 Ovington J.D. (1957) Dry-matter production by *Pinus sylvestris* L. *Annals of Botany*
45
46 667 XXI:288-314
47
48
49
50 668
51
52 669 Roberts J.M. (1976) A study of root distribution and growth in a *Pinus sylvestris* L.
53
54 670 (scots pine) plantation in East Anglia. *Plant and Soil* 44:607-621
55
56
57
58 671
59
60

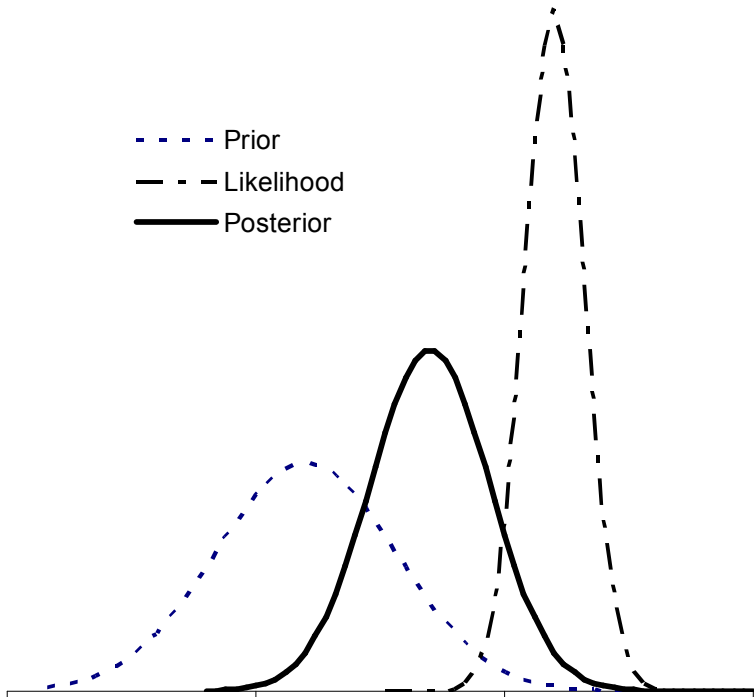
- 1
2
3
4 672 Running S.W., Coughlan J.C. (1988) A general model of forest ecosystem processes
5
6 673 for regional applications I. Hydrological balance canopy gas exchange and
7
8 674 primary production processes. *Ecological Modelling* 42:125-154
9
10 675
11
12 676 Rowland C.S, Patenaude G., Balzter H., Dawson T.P., Hill R.A., Luckman A., Milne
13
14
15 677 R., Skinner L. (2003) Forest carbon estimation: a comparison of techniques,
16
17 678 annual meeting of the Remote Sensing and Photogrammetry Society.
18
19
20 679
21
22 680 Sands P.J. (2004) Adaptation of 3-PG to novel species : guidelines for data collection
23
24
25 681 and parameter assignment. *Technical Report. No. 141*, CSIRO, CRC
26
27 682 Sustainable Production Forestry, Hobart
28
29 683
30
31 684 Sands P.J., Landsberg J.J. (2002) Parameterisation of 3-PG for plantation grown
32
33
34 685 Eucalyptus globulus. *Forest Ecology and Management* 163:273-292
35
36 686
37
38 687 Skinner L., Luckman A. (2000) Thetford forest ground data collection campaign in
39
40
41 688 support of the SHAC SAR acquisition, June 2000, University of Wales
42
43 689 Swansea, Swansea, Unpublished report 34p.
44
45
46 690
47
48 691 Stape J.L., Ryan M.G., Binkley D. (2004) Testing the utility of the 3-PG model for
49
50
51 692 growth of Eucalyptus grandis X urophylla with natural and manipulated
52
53 693 supplies of water and nutrients. *Forest Ecology and Management* 193:219-234
54
55 694
56
57
58
59
60

- 1
2
3 695 Stenberg P., Kuuluvainen T., Kellomaki S., Grace J.C., Jokela E.C., Gholz H.L.
4
5
6 696 (1994) Crown structure, light interception and productivity of pine trees and
7
8 697 stands. *Ecological Bulletins* 43:20-34
9
10 698
11
12 699 Stewart J.B. (1988) Modeling Surface Conductance of Pine Forest. *Agricultural and*
13
14 700 *Forest Meteorology* 43:19-35
15
16
17 701
18
19 702 Vanclay J.K. (1989) A growth model for North Queensland rainforests. *Forest*
20
21 703 *Ecology and Management* 27:245-271
22
23
24 704
25
26 705 van Hees A.F.M., Bartelink H.H. (1993) Needle Area Relationships of Scots Pine in
27
28 706 the Netherlands. *Forest Ecology and Management* 58:19-31
29
30
31 707
32
33 708 Van Oijen M., Rougier J., Smith R. (2005) Bayesian calibration of process-based
34
35 709 models: bridging the gap between models and data. *Tree Physiology* 25 (7):
36
37 710 915-927
38
39
40 711
41
42 712 Wang K.Y., Kellomaki S., Zha T.S., Peltola H. (2004) Component carbon fluxes and
43
44 713 their contribution to ecosystem carbon exchange in a pine forest: an
45
46 714 assessment based on eddy covariance measurements and an integrated model. .
47
48 715 24:19-34
49
50
51 716
52
53 717 Wang Y.P., Jarvis P.G. (1990) Description and Validation of an Array Model -
54
55 718 Maestro. *Agricultural and Forest Meteorology* 51:257-280
56
57
58 719
59
60

- 1
2
3
4 720 Waring R.H. (2000) A process model analysis of environmental limitations on the
5
6 721 growth of Sitka spruce plantations in Great Britain. *Forestry* 73:65-79
7
8 722
9
10 723 Waring R.H., Running S.W. (1998) *Forest ecosystems : analysis at multiple scales*,
11
12 724 2nd Ed. Academic Press, London 270 p.
13
14 725
15
16
17 726 White J.D., Coops N.C., Scott N.A. (2000) Estimates of New Zeland forest and scrub
18
19 727 biomass from the 3-PG model. *Ecological Modelling* 131:175-190
20
21
22 728
23
24
25
26
27
28
29
30
31
32
33
34
35
36
37
38
39
40
41
42
43
44
45
46
47
48
49
50
51
52
53
54
55
56
57
58
59
60

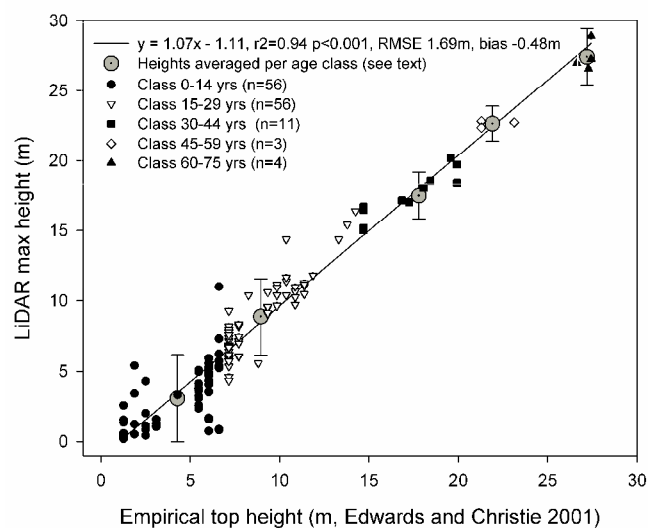
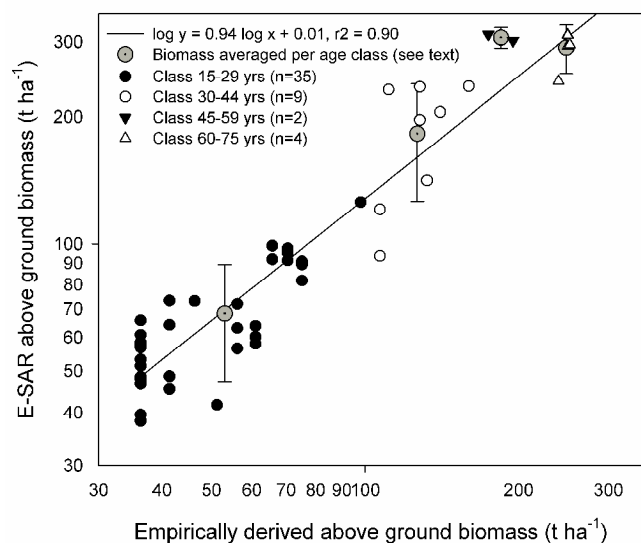
1
2
3
4
5
6
7
8
9
10
11
12
13
14
15
16
17
18
19
20
21
22
23
24
25
26
27
28
29
30
31
32
33
34
35
36
37
38
39
40
41
42
43
44
45
46
47
48
49
50
51
52
53
54
55
56
57
58
59
60

Figure 1



Review Only

Figure 2



Manuscript Only

1
2
3
4
5
6
7
8
9
10
11
12
13
14
15
16
17
18
19
20
21
22
23
24
25
26
27
28
29
30
31
32
33
34
35
36
37
38
39
40
41
42
43
44
45
46
47
48
49
50
51
52
53
54
55
56
57
58
59
60

Figure 3

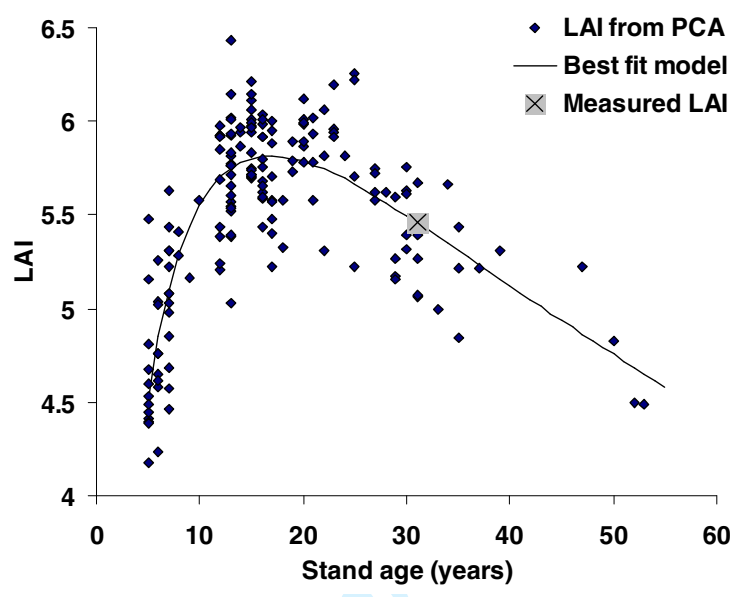
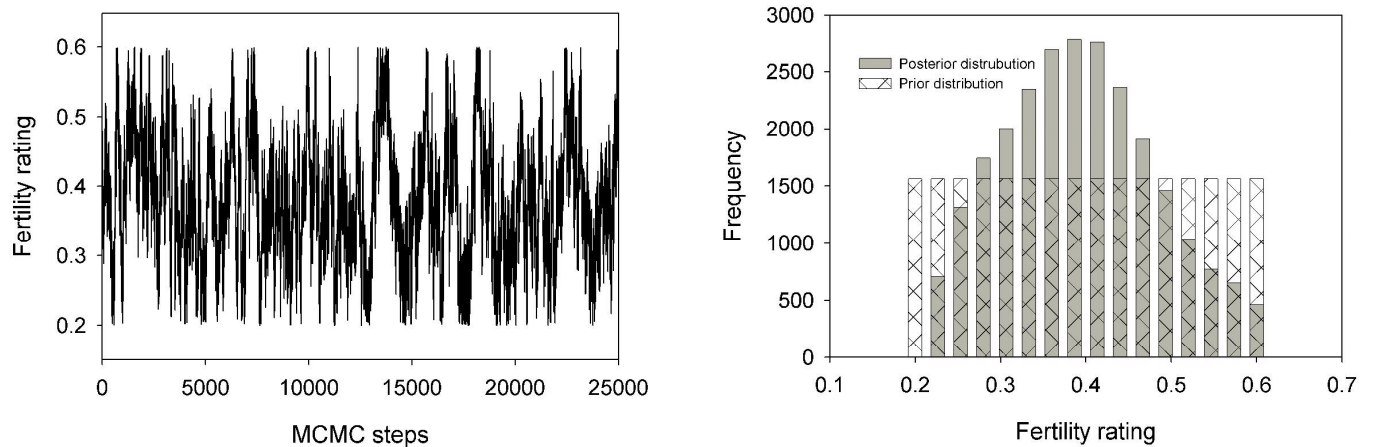


Figure 4



Peer Review Only

Figure 5

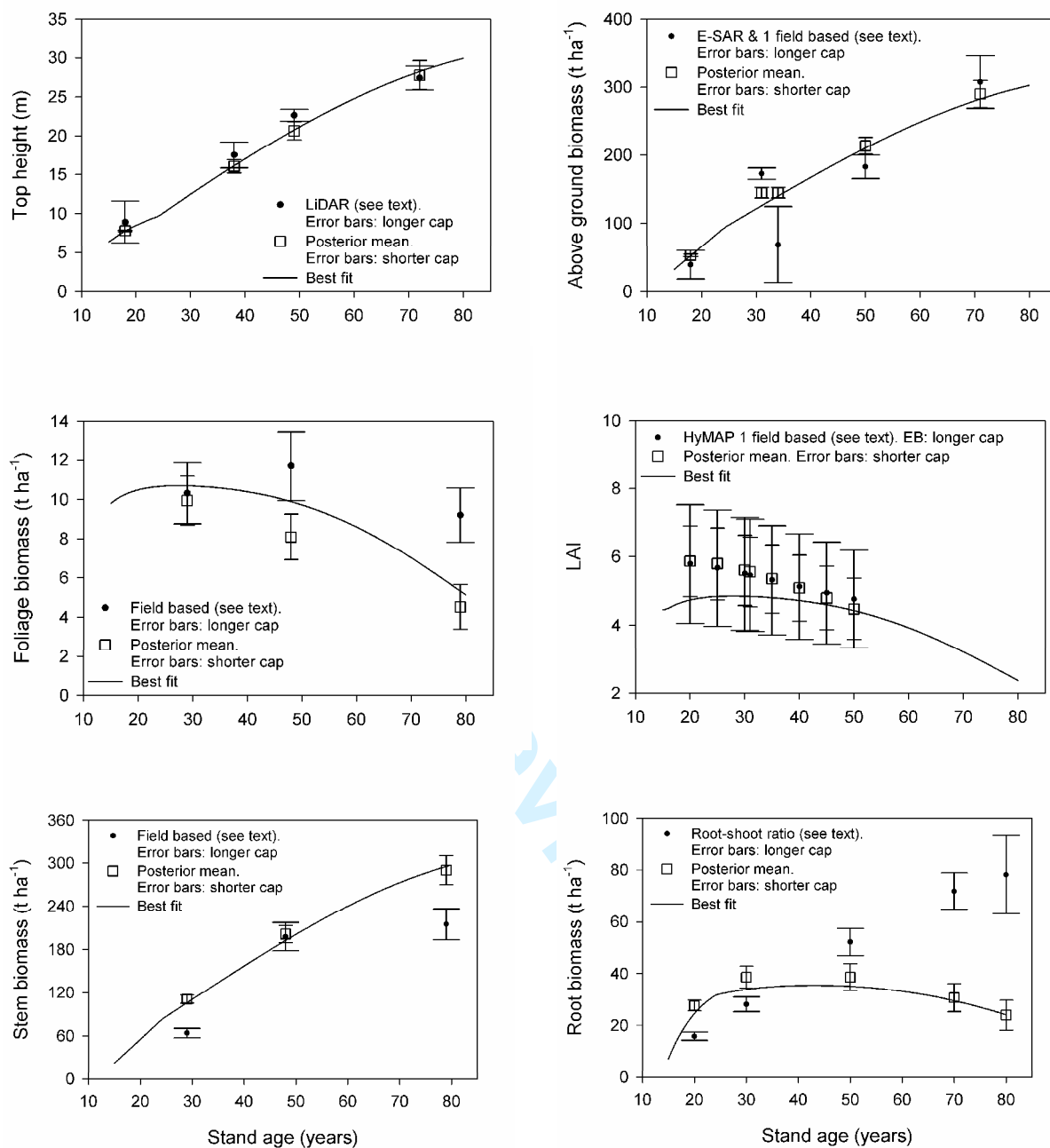
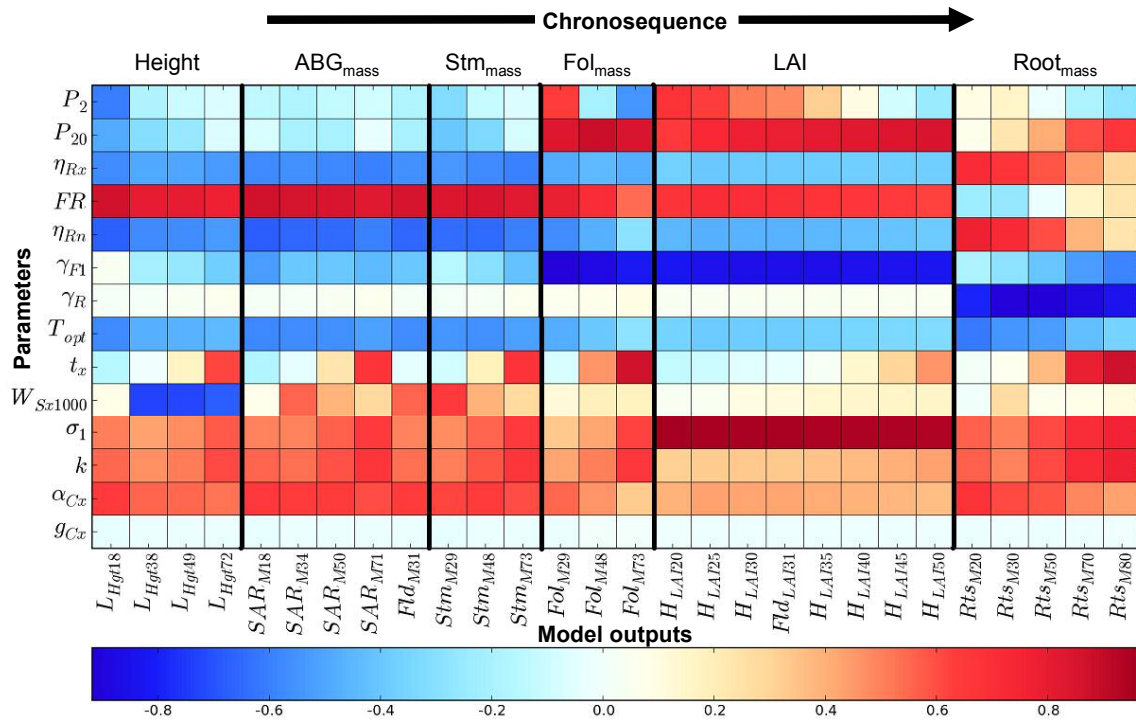


Figure 6:



GREY VERSION (if colour printer unavailable)

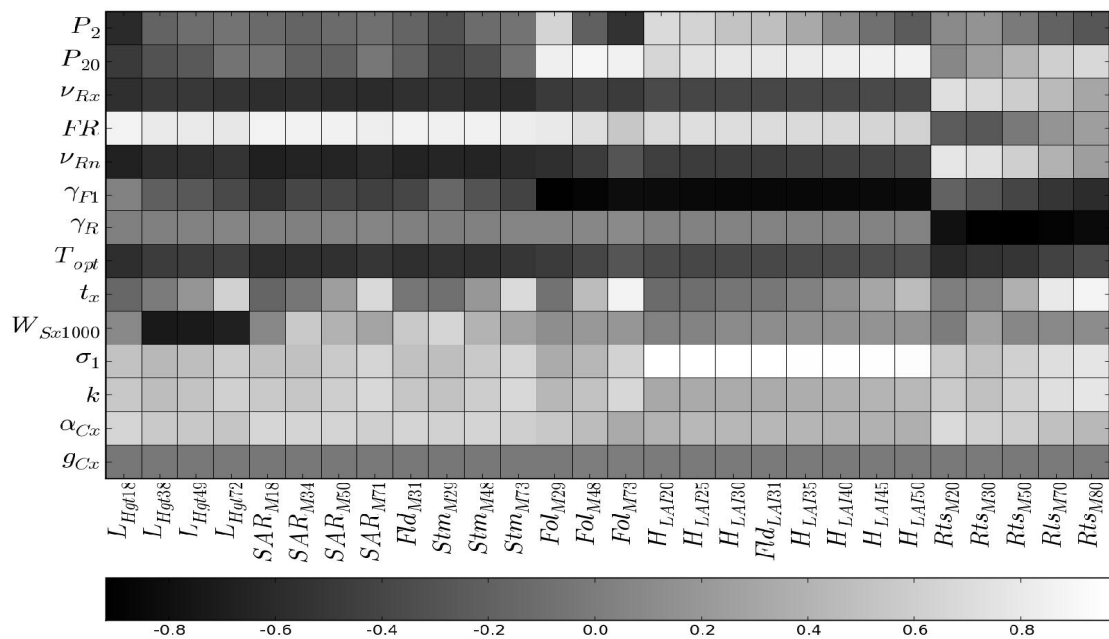


Table 1:

Monthly Climate data	Mean Tmax ^a (°C)	Mean Tmin ^a (°C)	Rain ^b (mm)	Solar rad ^b (MJ m ⁻² d ⁻¹)	Frost days ^a (days)
January	6.47	1.08	55.0	2.52	10.7
Feb	7.29	0.97	42.4	4.53	11.2
March	10.18	2.13	51.9	8.26	7.9
April	13.13	3.95	48.0	13.10	3.3
may	16.86	6.70	55.0	16.58	0.8
June	20.08	9.73	55.0	18.43	0.0
July	22.31	11.83	54.0	16.64	0.0
Aug	22.15	11.58	58.0	14.42	0.0
Sep	19.17	9.64	61.1	10.00	0.0
Oct	14.99	6.66	61.1	5.80	1.5
Nov	10.07	3.51	69.0	2.86	5.7
Dec	12.61	2.04	61.1	1.96	9.1

Table 2

3-PG symbol: Description (units)	S Class ^a	Prescribed Parameter Values	Calibrated Parameters: ranges of values in the prior		Data Class ^b	Source/Comment
			θ_{min}	θ_{max}		
a_S : Constant in stem mass ν diam. relationship	M	0.02	-	-	CP-T	Baker 1992, Baker <i>et al.</i> 1994, Edwards and Christie 1981.
c_θ : Moisture ratio deficit which gives $f_\theta = 0.5$	H	0.7	-	-	D	Default for sandy soils
f_{N0} : Value of f_N when $FR = 0$	M	0.6	-	-	D	
FR : Fertility rating	?	-	0.2	0.6	CP-T	Soil Fertility (Corbett 1973, Roberts <i>et al.</i> 1982)
g_B : Canopy boundary layer conductance ($m\ s^{-1}$)	L	0.2	-	-	D	
g_{Cx} : Maximum canopy conductance ($m\ s^{-1}$)	H	-	0.015	0.03	P-L	Kelliher <i>et al.</i> 1995
i_{Rx} : Maximum fraction of rainfall intercepted by canopy	M	0.15	-	-	D	
k : Extinction coefficient for PAR absorption by canopy	M	-	0.4	0.7	P-L	Stenberg <i>et al.</i> 1994, Mencuccini and Grace 1996
k_F : Number of days production lost for each frost day	L	1	-	-	D	
L_{Cx} : Canopy LAI for maximum canopy conductance ($m^2\ m^{-2}$)	L	3.33	-	-	P-L	Kelliher <i>et al.</i> 1995, Mencuccini and Grace, 1996
L_{ix} : LAI for maximum rainfall interception ($m^2\ m^{-2}$)	L	0	-	-	D	
m_θ : Value of m when $FR = 0$?	0	-	-	D	
m_F : Fraction of mean foliage biomass per dying tree	L	0	-	-	D	
m_R : Fraction of mean root biomass per dying tree	L	0.2	-	-	P-L	Empirical data (Edwards and Christie 1981, Ovington 1957)
m_S : Fractions of mean stem biomass per dying tree	L	0.2	-	-	CP-L	Empirical data (Edwards and Christie 1981)
n_{age} : Power of relative age in f_{age}	L	4	-	-	D	
n_N : Power in self thinning law	L	1.5	-	-	P-L	Theoretical scaling laws & observation
n_{fN} : Power of $(1-FR)$ in f_N	L	1	-	-	D	
n_S : Power in stem mass ν diam. Relationship	H	2.88	-	-	CP-T	Baker 1992, Baker <i>et al.</i> (1994), Edwards and Christie 1981

n_{ϕ} : Power of moisture ratio deficit in f_{ϕ}	L	9	-	-	D	Default for sandy soils
p_2 : Ratio of foliage:stem partitioning at $B = 2$ (cm)	H	-	0.5	1	P-L	Gower <i>et al.</i> 1994
p_{20} : Ratio of foliage:stem partitioning at $B = 20$ (cm)	H	-	0.1	0.5	P-L	Gower <i>et al.</i> 1994
p_{BB0} : Branch and bark fraction at stand age 0	L	0.5	-	-	P-L	Default 3-PG values for P.radiata
p_{BB1} : Branch and bark fraction for mature aged stands	L	0.1	-	-	P-L	Default 3-PG values for P.radiata
r_{age} : Relative age to give $f_{age} = 0.5$	L	0.95	-	-	D	
t_{BB} : Age at which $p_{BB} = \frac{1}{2}(p_{BB0} + p_{BB1})$	L	5	-	-	P-L	Default 3-PG values for P.radiata
t_c : Age at full canopy cover (yr)	M	0	-	-	P-L	
T_{max} : Maximum temperature for growth ($^{\circ}\text{C}$)	L	35	-	-	P-L	
T_{min} : Minimum temperature for growth ($^{\circ}\text{C}$)	L	0	-	-	D	
T_{opt} : Optimum temperature for growth ($^{\circ}\text{C}$)	M	-	18	22	P-L	Waring and Running, 1998
t_x : Maximum stand age used to compute relative age (year)	L	-	60	100	D	10% of age at maximum height (Waring, pers. Comm.)
$t_{\gamma F}$: Age at which litterfall rate has median value (month)	L	36	-	-	D	
t_{σ} : Age at which specific leaf area = $\frac{1}{2}(\sigma_0 + \sigma_1)$ (yr)	L	2.5	-	-	D	
W_{Sx1000} : Maximum stem mass per tree at 1000 trees/ha	-	-	160	400	CP-L	live stem numbers time-series: Edwards and Christie (1981)
Y : Ratio NPP/GPP	H	0.47	-	-	P-L	Waring & Running (1998)
α_{Cx} : Maximum canopy quantum efficiency (mol mol^{-1})	H	-	0.045	0.065	P-L	Range for temperate species in 3-PG (e.g. Stenberg <i>et al.</i> 1994, Law <i>et al.</i> 2000, Waring 2000, Waring <i>et al.</i> 2002, Wang <i>et al.</i> 2004)
γ_{F0} : Litterfall rate at $t = 0$ (month^{-1})	L	0.001	-	-	D	
γ_{F1} : Litterfall rate for mature stands (month^{-1})	H	-	0.025	0.035	P-T	Beadle <i>et al.</i> 1982, Cousens (1988)
γ_R : Average monthly root turnover rate (month^{-1})	L	-	0.006	0.015	P-L	Gill & Jackson (2000)
η_{Rn} : Minimum fraction of NPP to roots	M	-	0.20	0.50	P-T	Ovington (1957), Levy <i>et al.</i> (2004)
η_{Rx} : Maximum fraction of NPP to roots	M	-	0.50	0.80	P-T	Ovington 1957, Levy <i>et al.</i> (2004)
σ_0 : Specific leaf area at stand age 0 ($\text{m}^2 \text{kg}^{-1}$)	L	5	-	-	P-L	VanHees & Bartelink (1993)
σ_1 : Specific leaf area for mature aged stands ($\text{m}^2 \text{kg}^{-1}$)	H	-	4	8	P-L	VanHees & Bartelink (1993)
ρ_l : Basic density	H	0.43	-	-	CP-L	Hamilton (1975)

Table 3:

$\theta(i)$	$\overline{\theta(i)}$	SD	θ_{MAPx}
<i>FR</i>	0.380	0.090	0.391
<i>g_{Cx}</i>	0.023	0.004	0.023
<i>K</i>	0.539	0.087	0.439
<i>p₂</i>	0.694	0.133	0.502
<i>p₂₀</i>	0.441	0.045	0.497
<i>T_{opt}</i>	20.893	0.911	20.42
<i>t_x</i>	90.656	6.978	95.86
<i>w_{Sx1000}</i>	182.826	17.504	165.0
<i>α_{Cx}</i>	0.047	0.002	0.046
<i>γ_{F1}</i>	0.028	0.003	0.026
<i>γ_R</i>	0.013	0.002	0.013
<i>η_{Rn}</i>	0.237	0.028	0.221
<i>η_{Rx}</i>	0.580	0.067	0.557
<i>σ_l</i>	5.711	1.029	4.539

1
2
3
4
5
6
7
8
9
10
11
12
13
14
15
16
17
18
19
20
21
22
23
24
25
26
27
28
29
30
31
32
33
34
35
36
37
38
39
40
41
42
43
44
45
46
47
48
49
50
51
52
53
54
55
56
57
58
59
60

For Peer Review Only